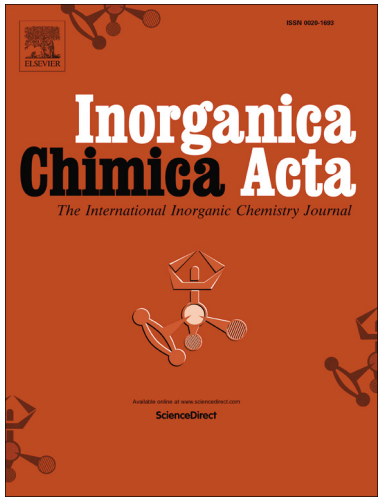

Non-Innocent Ground State Electronic Structure of a Polynuclear Copper Complex with Picolinate Bridges

Róbert Csonka, Dóra Lakk-Bogáth, Ágnes Gömöry, László Drahos, Michel Giorgi, Gábor Speier, Róbert K. Szilágyi, József Kaizer

PII: S0020-1693(17)30448-6
DOI: http://dx.doi.org/10.1016/j.ica.2017.07.065
Reference: ICA 17788

To appear in: *Inorganica Chimica Acta*

Received Date: 22 March 2017
Revised Date: 27 June 2017
Accepted Date: 31 July 2017

Please cite this article as: R. Csonka, D. Lakk-Bogáth, A. Gömöry, L. Drahos, M. Giorgi, G. Speier, R.K. Szilágyi, J. Kaizer, Non-Innocent Ground State Electronic Structure of a Polynuclear Copper Complex with Picolinate Bridges, *Inorganica Chimica Acta* (2017), doi: http://dx.doi.org/10.1016/j.ica.2017.07.065

Non-Innocent Ground State Electronic Structure of a Polynuclear Copper Complex with Picolinate Bridges

Róbert Csonka,[a] Dóra Lakk-Bogáth,[a] Ágnes Gömöry,[b] László Drahos,[b] Michel Giorgi,[c] Gábor Speier,[a] Róbert K. Szilágyi,[d,*] József Kaizer[a,*]

[a] *Department of Chemistry, University of Pannonia, 8201 Veszprém, Hungary.*

[b] *Hungarian Academy of Sciences, Research Centre for Natural Sciences, H-1117 Budapest, Hungary*

[c] *Aix Marseille Université, CNRS, Centrale Marseille, Spectropole FR1739, 13397 Marseille, France*

[d] *Department of Chemistry & Biochemistry, Montana State University, Bozeman, MT 59717, USA*

Abstract

A mononuclear copper complex $[Cu^{II}(asN4Py)(MeCN)](O_3SCF_3)_2$ (**1**) and its mixed mono- and trinuclear $[Cu(pic)_2(ClO_4)_2][Cu_3(asN4Py)_2(pic)_2(ClO_4)_2](ClO_4)$ derivatives (**2**) were synthesized containing *N*,*N*-bis(2-pyridylmethyl)-1,2-di(2-pyridyl)-ethylamine (asN4Py) chiral ligands and 2-picolinate (pic) bridges. The structures were elucidated using single crystal X-ray diffraction and spectroscopic methods. Due to the non-trivial assignments of the formal Cu oxidation states, the d-electron count and the location of electron holes were assigned by broken-symmetry electronic structure calculations using a spectroscopically validated, hybrid density functional theory with saturated basis set. The ground state description of the mononuclear complexes is trivial; thus, they were used to validate the computational level of theory and the modelling approach. The experimental structure of the trinuclear complex can only be described by considering two asymmetric resonance structures in the crystal structure containing Cu^{II}-Cu^{II}-Cu^{I}/Cu^{I}-Cu^{II}-Cu^{II} metal centres.

Keywords: Copper(II); Pentadentate; Chiral; X-ray crystal structure; Computation.

---

*To whom correspondence should be addressed. Address: Department of Chemistry, University of Pannonia, H-8201 Veszprém, Wartha V. u. 1., Hungary. E-mail: kaizer@almos.vein.hu. Tel.: (+36)88624720.

1. Introduction

The unique electron donating properties of multidentate *N*-donor ligands have been successfully exploited in the past few decades. This ligand class in enzyme mimics has a specific role, due to their capability of maintaining high-valent oxidation states of transition metal ions even at mild conditions with considerable stability [1,2]. In the enzymatic cycle of iron dependent oxidoreductases, oxoiron(IV) [3] or oxoiron(V) [4] species were found to be responsible for catalytic activity. In order to investigate directly these short lived intermediates tridentate (e.g. BnBQA - *N*-benzyl-*N*,*N*-di(quinolin-2-ylmethyl) amine) [5] tetradentate (e.g. TPA - tris-(2-pyridylmethyl)amine) [6], and pentadentate (e.g. N4Py - *N*,*N*-bis(2-pyridylmethyl)-*N*-bis(2-pyridyl)methylamine) [7] ligands were synthesized. Complexes containing these ligands often participate in hydrogen atom transfer (HAT) and oxygen atom transfer (OAT) reactions that adequately mimic enzymatic processes [8].

Recently, the synthesis of *N*,*N*-bis(2-pyridylmethyl)-1,2-di(2-pyridyl)-ethylamine (asN4Py), a chiral derivative of the pentadentate N4Py was reported [9]. The introduction of an additional methylene group into the ligand architecture greatly increases the lifespan of the oxoiron(IV) species formed from the $[Fe^{II}(asN4Py)]^{2+}$ precursor complex. However, its reactivity in thioanisole oxidation, for example, partially diminished. The enantiomeric excess (*ee*) of 87% was achieved by metal-based oxidation of 4-MeO-PhSMe [9]. With relevance to the given work, dioxygen activation during the oxidation of thioanisoles, alcohols, or even alkanes is also commonly catalysed by both copper(II) or copper(I) complexes [10,11].

In order to extend the number of chiral transition metal complexes suitable for mimicking HAT or OAT enzymatic reactions, we synthesized two new copper complexes with asN4Py ligand: $[Cu^{II}(asN4Py)(MeCN)](OTf)_2$ (**1**) and its polynuclear counterpart $[Cu(pic)_2(ClO_4)_2][Cu_3(asN4Py)_2(pic)_2\ (ClO_4)_2](ClO_4)$ (**2**). Both complexes were characterized by single crystal X-ray crystallography (SCXRD), electrospray ionization mass spectrometry (ESI-MS), cyclic voltammetry (CV), ultraviolet-visible (UV-vis), and infrared spectroscopy (IR). Furthermore, ^{18}O labelled dioxygen uptake experiments were carried out to confirm O_2 insertion into complex **2**.

Complexes **1** and **2** were synthesized as part of our ongoing research in Baeyer-Villiger oxidation (BVO) reaction of cyclohexanones in the presence of transition metal complexes, where cycloketones can be transformed to the corresponding lactone by an aldehyde/O_2 oxidant system *via in situ* generated percarboxylic acid [12]. To date the title complexes **1** and **2** were found to be inactive in BVO reaction; however, the oxidation of a coordinated aldehyde (2-pyridinecarboxaldehyde, in the given case) was observed.

Remarkably, complex **2** poses an ambiguous oxidation state assignment due to the simultaneous presence of mono- and trinuclear Cu complexes in the asymmetric unit and the presence of a non-coordinated perchlorate counter ion. The ambiguity in the electronic structure was addressed here by a detailed computational study that defined the most reasonable location and distribution of the copper 3d electron holes for the trinuclear complex. The employed computational approach has recently been successfully utilized for describing the ground state of a trinuclear Cu^{II} complex with biomimetic catecholase function [13]. The level of theory was selected to be a hybrid density functional that gives experimentally sound ground-state description for Cu^{II}/Cu^{I} complexes [14-17]. Validation for the given complexes was carried out using the electronically and structural well-defined complex **1** with a formally Cu^{II} site. The structural changes among Cu^{I}, Cu^{II}, and Cu^{III} formal oxidation states provided the basis for differentiating among various oxidation and spin state assignments for the mono- and trinuclear components of **2**.

2. Results and discussion

*Characterization of complex **1***. The racemic mixture of asN4Py ligand with $Cu^{II}(OTf)_2$ salt in dry acetonitrile forms the monomer complex **1** according to the equation: $[Cu^{II}(OTf)_2]$ + asN4Py → $[Cu^{II}(asn4Py)(MeCN)](OTf)_2$. SCXRD analysis from blue, cubic crystals revealed a disordered octahedral coordination environment around the Cu^{II} centre in **1** (Figure 1) as expected based on the structure of other N4Py complexes [2,7,18].

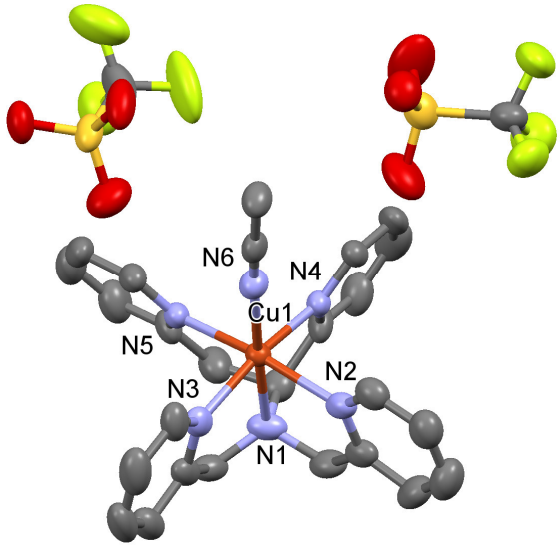

Fig. 1. Crystal structure of complex **1**. Thermal ellipsoids are plotted at 50% probability level. Hydrogen atoms were omitted for clarity. (CCDC 1516132).

The ligand asN4Py coordinates five N-atoms to the Cu^{II}, while the sixth coordination site is occupied by an acetonitrile solvent molecule. The outer sphere consists of two triflate $(OTf)^-$ anions. Table 1 summarizes the distinctive lengths of the Cu-N(pyridine), Cu-N(axial ligand), Cu-N(amine) bonds. It is remarkable to note that the insertion of a methylene group in asN4Py to create a chiral environment for **1** causes a considerable change of the Cu-N distances in comparison to the symmetric $[Cu^{II}(N4Py)(NO_3)](NO_3)$ complex [18]. This is compounded by the presence of an inner sphere coordinated anionic ligand in the latter. Due to these differences, the $Cu\text{-}N_{py}$ bonds shorten by 0.10 Å on average, while the axial $Cu\text{-}N_{amine}$ bond elongates by 0.04 Å in **1** *versus* its symmetric analogue (Table 1). The axial $Cu\text{-}N_{MeCN}$ distance also elongates by 0.14 Å compared to the anionic $(NO_3)^-$ ligand in $[Cu^{II}(N4Py)(NO_3)](NO_3)$. Despite the asymmetry, the overall coordination geometry of **1** appears to be more balanced, as can be judged from the similar Cu-N distances and close to ideal N-Cu-N bond angles. This indicates the lack of significant strain caused by the insertion of a methylene group in asN4Py relative to N4Py ligand.

Table 1. Comparison of different Cu-N bond distances (Å) for various Cu(N4Py) derivatives.

complexes	$M–N_{py}$ (avg.)	$M–N_{MeCN}$ (or axial L)	$M–N_{amine}$	Ref.
$[Cu^{II}(N4Py)(NO_3)](NO_3)$	2.207	1.991(3)	2.095	[13]
1	2.112	2.130(3)	2.138(3)	this work
2	2.067	1.945(2)	2.028(2)	this work

The negative and positive ESI mass spectra (Figure 2) show the corresponding single charged molecule ions of **1**. The peaks at *m/z* = 891.3 and 593.1 can be assigned to $[Cu^{II}(asN4Py)(OTf)_3]^-$ (z=1) (calcd.: 890.98) and $[Cu^{II}(asN4Py)(OTf)]^+$ (z=1) (calcd.: 593.08), respectively.

The electrochemical properties of **1** were determined from cyclic voltammetric measurements in acetonitrile solution (Figure 3). The $Cu^{II/I}$ couple was found to be chemically reversible at the potential of E^0 = +0.063 V, similar to that of $[Cu^{II}(N4Py)(NO_3)](NO_3)$ (E^0 = -0.05 V). A similar qualitative difference (E^0 = 600 mV) in half-cell potentials was observed for the Fe(N4Py) and Fe(asN4Py) complexes containing the same types of ligands.

Copper(II) complexes often exhibit broad UV-vis bands with low intensity at longer wavelengths than the 600 nm region [19,20]. The characteristic d-d transition region consists of two bands in case of **1** at 632 nm (= 78 M^{-1} cm^{-1}) and 852 nm (= 127 M^{-1} cm^{-1}). EPR data

of powder and solution samples (A_0 = 54.6(2) G, α = 51.4(5) G, β = -6.4(2) G, γ = -0.2(1) G.) are consistent with the proposed structure (Figure 4).

The C=N bond stretching in the IR spectrum (see experimental part) is associated with the strong band at 1608 cm^{-1}. Furthermore, the breathing mode of the pyridine ring at 1030 cm^{-1} indicates the coordination of this group to the metal centre. Two bands at 1274 cm^{-1} and 638 cm^{-1} are associated with the non-coordinated triflate anions.

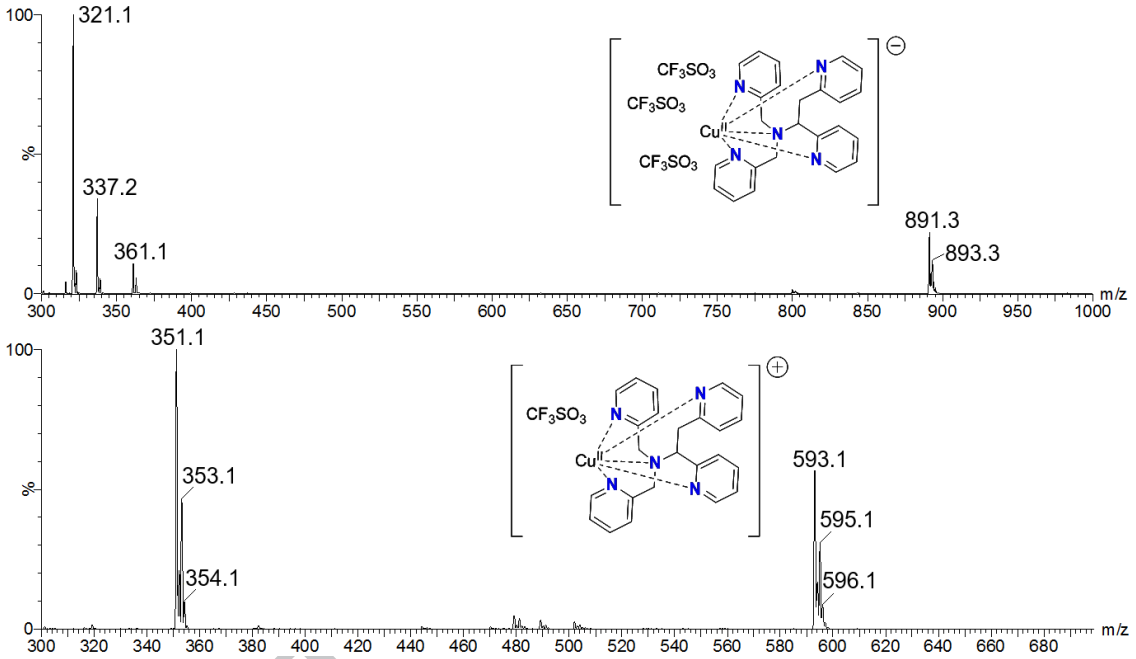

Fig. 2. Electrospray ionization mass spectrum of **1**. The peaks at *m/z* values 891.3 and 593.1 correspond to the negative (top) and positive (bottom) ESI-MS formulae of the complex: $[Cu^{II}(asN4Py)(OTf)_3]^-$ (z=1) and $[Cu^{II}(asN4Py)(OTf)]^+$ (z=1), respectively.

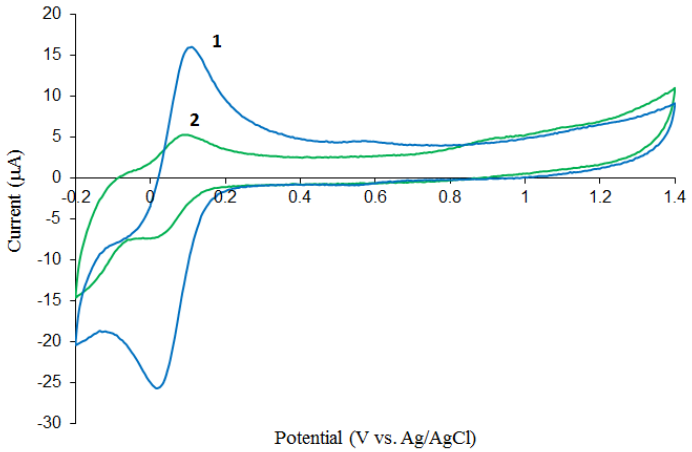

Fig. 3. Cyclic voltammograms of **1** and **2** (1 mM) in CH_3CN with 0.1 M $(Bu_4N)ClO_4$; scan rate 100 mVs^{-1}; working electrode: glassy carbon electrode (GCE), auxiliary electrode: Pt wire, reference electrode: Ag/AgCl.

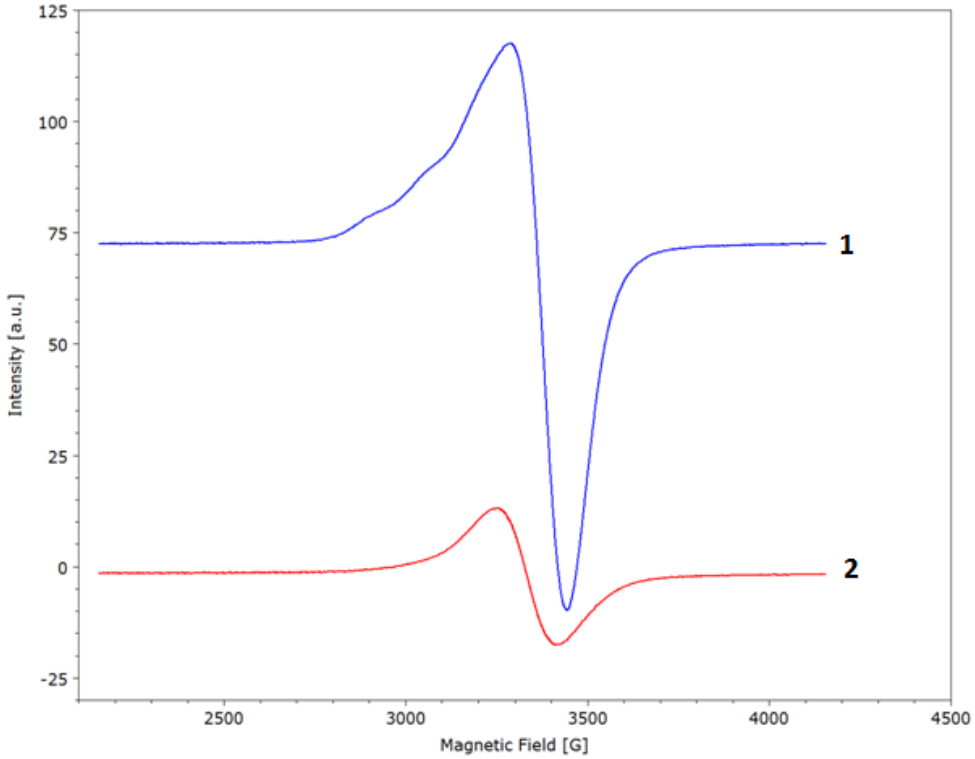

Fig. 4. Solid EPR spectra of **1** and **2**.

Formation and characterization of complex ***2****.* Stirring the copper salt $Cu^{I}(CH_3CN)_4ClO_4$, asN4Py ligand, and the pyridinecarboxaldehyde (picAld) in acetonitrile at room temperature for 1 hr in air atmosphere, followed by two days of crystallization resulted in the formation of **2** according to the reaction 4 $[Cu(CH_3CN)_4](ClO_4)\times HClO_4$ + 2 asN4Py + 4 picAld + 2 O_2 → $[Cu_4(asN4Py)_2(pic)_4(ClO_4)_4](ClO_4)$ (**2**). As discussed later, the actual formation reaction is more complex given the protonated state of the pyridine rings of the asN4Py ligand and the presence of a non-coordinating $(ClO_4)^-$ anion. Single-crystal X-ray diffraction (SCXRD) measurements revealed a polynuclear composition with mono- (Figure 5, top) and trinuclear components (Figure 5, bottom). Notably, one of the pyridyl arms in **2** remains detached from the copper ion with a trigonal bipyramidal environment (τ = 0.70) [21]. The coordination of the pyridine is further hindered by its protonated state as confirmed by SCXRD data. There is an uncoordinated $(ClO_4)^-$ anion in the asymmetric unit, which hints a more complex redox reaction during formation of **2** than expressed by the above equation. The copper ions in the

trinuclear moiety of **2** are held together by picolinate bridges with Cu-O(pic) distances of 1.945 Å and 1.968 Å. The peripheral Cu(asN4Py) moieties of the trinuclear complex in **2** show a considerable deviation of -0.14 Å and -0.07 Å from $[Cu^{II}(N4Py)(NO_3)](NO_3)$ when considering average Cu-N_{py} and Cu-N_{amine} distances of 2.067 Å and 2.028 Å, respectively (Table 1); while the axial Cu-O interactions agree reasonably well within 0.04 Å.

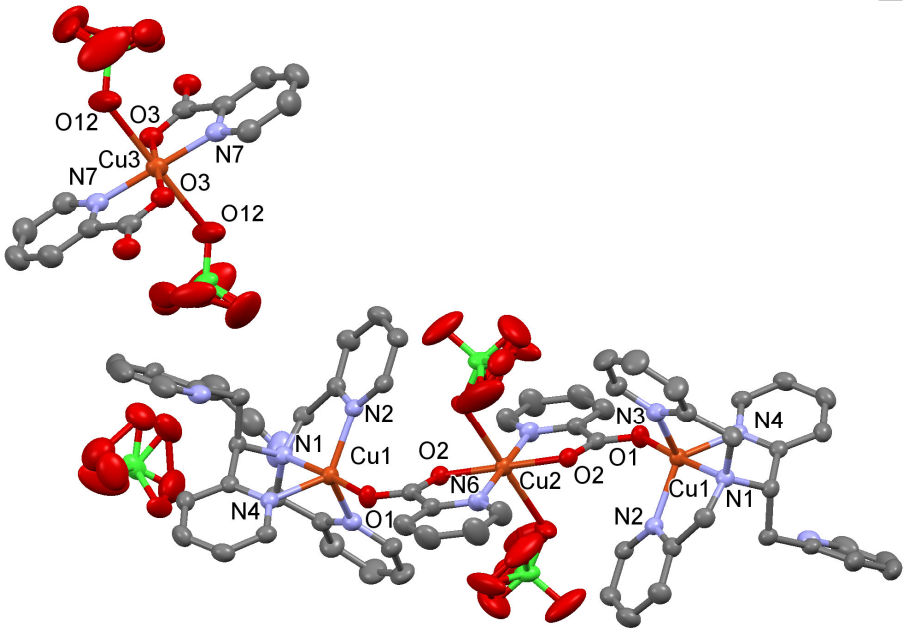

Fig. 5. Crystal structure of complex **2**. Thermal ellipsoids are plotted at 50% probability level. Hydrogen atoms were omitted for clarity. (CCDC 1516133).

In the electronic absorption spectrum of **2** (Figure 6), the expected red-shift of d-d transition was observed with slightly higher molar absorption coefficients (670 nm, = 210 M^{-1} cm^{-1}. This absorption is characteristic to a five coordinated copper geometry. It is also important to point out that the d-d bands in the spectrum of **2** are coming from four different Cu absorbers. The broad singlet signal in the solid EPR spectrum may be explained by a dipole-dipole interaction of Cu(II) centres in the Cu(II)-Cu(II)-Cu(I) complex (**2**) (Figure 4). The electrochemical properties of **2** were also determined from cyclic voltammetric measurements in acetonitrile solution (Figure 3). $Cu^{II/I}$ couple was found to be chemically reversible at the potential of E^0 = +0.060 V. This value is very similar to that of **1**, which may be explained by the dissociation of **2** in the presence of excess of $(Bu_4N)ClO_4$ salt.

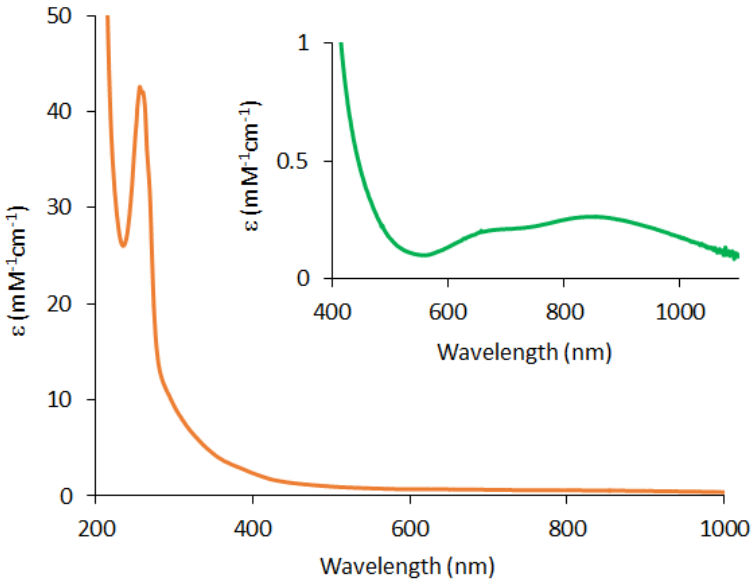

Fig. 6. UV−Vis spectra of complex **2** in acetonitrile recorded at room temperature (298 K).

In order to gain insights into the formation of **2**, the oxidation and insertion of 2-pyridinecarboxaldehyde was followed by dioxygen uptake measurements using gas volumetry and ^{18}O labelling and concomitant ESI-MS and FTIR analysis. Figure 7 shows that 0.5 mmol O_2/Cu; picAld is needed for the formation of **2** as required by the chemical equation shown above. Based on this stoichiometry, an *in situ* generation of dipicolylperoxide can be proposed to be a key intermediate during oxidation.

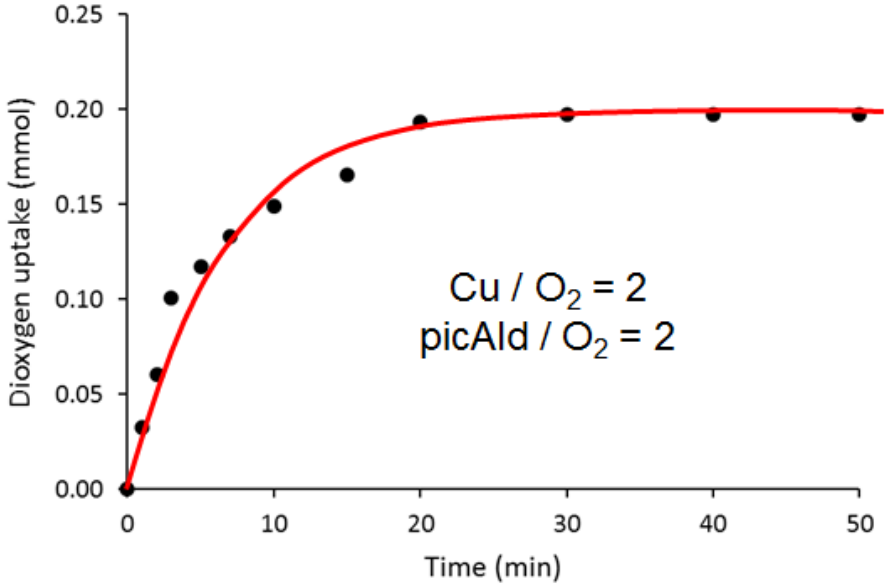

Fig. 7. Dioxygen uptake during complex **2** formation. $Cu(MeCN)_4ClO_4$ = 0.4 mmol, 2-pyridinecarboxaldehyde = 0.4 mmol, asN4Py = 0.2 mmol in MeCN at 303 K.

The molecular ion of the trinuclear fragment in ESI-MS spectra of labelled and non-labelled complex **2** show mass differences of 4 that correlates with the insertion of one molecule of O_2 (Figure 8). The formation of the mononuclear $[Cu(pic)_2(OTf)_2]$ moiety requires an additional molecule of O_2. A further evidence for the role of dioxygen was found by FTIR spectroscopy. Coordinated $\nu_{as}(COO^-)$ and $\nu_{sym}(COO^-)$ vibrations were assigned to 1638-1629 cm^{-1} and 1387-1354 cm^{-1} regions in picolinatocopper(II) complexes, respectively [22-24]. The double peaks in both regions can be assigned to the bridging ($\Delta\nu$ ~ 268 cm^{-1}) and non-bridging ($\Delta\nu$ ~ 243 cm^{-1}) carboxylate vibrations [25]. Small isotope shifts to lower wave numbers ($\Delta\nu$ = 8 cm^{-1} for asymmetric and $\Delta\nu$ = 8-11 cm^{-1} for symmetric vibrations) were detected in the ^{18}O labelled spectrum from 1630 cm^{-1} (^{16}O) to 1622 cm^{-1} (^{18}O) and 1387 cm^{-1} (^{16}O) to 1375 cm^{-1} (^{18}O) (Figure 9). Splitting of the broad bands at 1090 cm^{-1} and 1022 cm^{-1} indicates the presence of inner and outer-sphere perchlorates [26]. From a detailed study on the IR spectra of pyridinium salts and ions, the 3434 cm^{-1} region was assigned to the NH vibrations that are found in **2** with protonated pyridyl arms. The C=C and C=N stretching modes show twin bands at 1607 and 1590 cm^{-1} [27].

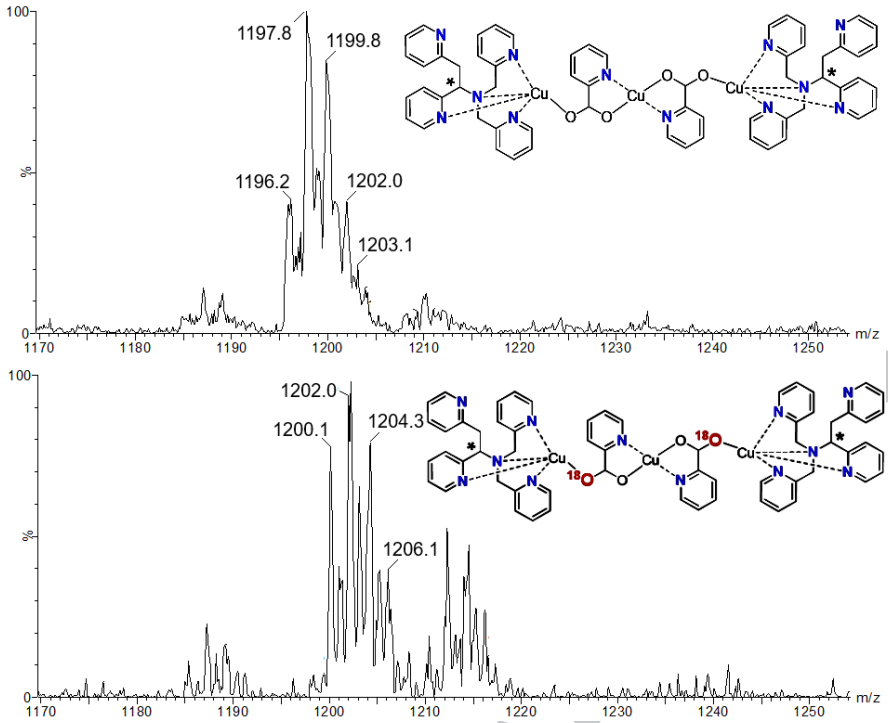

Fig. 8. Electrospray ionization mass spectrum of the trinuclear fragment of **2** (top) and ^{18}O labelled **2** (bottom). The peaks at *m/z* values 1197.8 and 1202.0 correspond to the formulae $[Cu_3(asN4Py)_2(pic)_2]^{3+}$ and $[Cu_3(asN4Py)_2(^{18}pic)_2]^{3+}$, respectively.

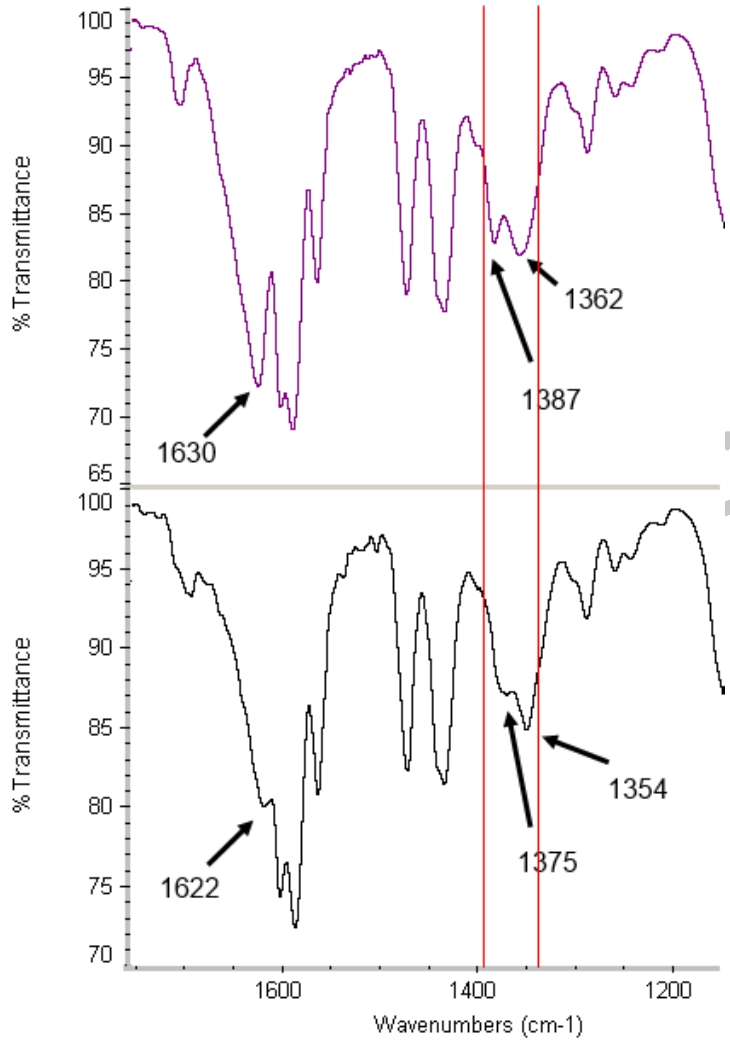

Fig. 9. FT-IR spectrum of **2**. (top) and its ^{18}O (bottom) derivate with the spectral change in $\nu(COO^{-})$ vibrations (in KBr pellets).

Using geometric criteria for assigning formal oxidation states. The well-defined ground state description of **1** provided us with the opportunity to evaluate the performance of the spectroscopically calibrated, hybrid density functional for a Cu^{II} complex with a weak/intermediate ligand field environment and low metal-ligand covalency. This is important, since the particular hybrid GGA functional used was developed for describing highly covalent Cu-Cl [14] and Cu-S [15] bonding. A validated level of theory has the decisive power for eliminating ambiguity in the Cu centre oxidation states of the mono- and trinuclear components in **2**, thus compare and contrast the adequacy of various oxidation and spin state assignments with respect of the SCXRD structure. The detailed numerical analyses for each comparison are provided as supporting information (Table S1), while Table 2

contrasts the root mean square (RMS) deviations in bond lengths and atomic positional coordinates for the inner and outer coordination spheres as a function of oxidation state assignments.

Table 2. Root mean square deviations (Å, weighted by the number of bond lengths for each type) between B(38HF)P86/def2TZVP calculated and experimental (SCXRD) bond lengths and atomic positional coordinates in gas phase, in condensed phase modeled by polarizable continuum model (CPCM) with acetonitrile (MeCN) and water (H_2O) parameters), and in presence of triflate (OTf^-) counter ions for complex **1**.

	gas phase				
	Cu^{I}	Cu^{II} S=1/2	Cu^{III} S=0	Cu^{III} S=1	$Cu^{(II)}$ S=1/2 w/$(OTf)^-$
bond lengths	0.58	0.09	0.23	0.05	0.05
Cu-N only	0.79	0.13	0.33	0.08	0.09
all positions	2.38	0.15	0.25	0.14	0.10
inner sphere	2.07	0.14	0.28	0.11	0.09

	Solution phase (CPCM)			
	$Cu^{(II)}$ S=1/2 MeCN	$Cu^{(II)}$ S=1/2 H_2O	$Cu^{(III)}$ S=0 MeCN	$Cu^{(II)}$ S=1/2 MeCN w/$(OTf)^-$
bond lengths	0.06	0.06	0.07	0.06
Cu-N only	0.10	0.10	0.12	0.09
all positions	0.13	0.13	0.13	0.12
inner sphere	0.11	0.12	0.11	0.10

It is evident from the first columns of Table 2 that the Cu^{I} oxidation state can be readily ruled out due to the close to 1 Å deviations in internal coordinates and more than 2 Å deviations in atomic positions. On the contrary, the optimized structures with Cu^{II} or Cu^{III} ion gave rather similar deviations from the SCXRD structure. One could argue that in the gas phase calculations without the presence of counter ions, the high spin Cu^{III} complex (Figure 10C) may even give a better agreement in bond lengths and atomic positions than the Cu^{II} complex (outer sphere: 0.05 vs. 0.09 Å; inner sphere: 0.08 vs. 0.13 Å, respectively). It is also evident that the consideration of low spin Cu^{III} formal oxidation state assignment does not result in an experimentally sound optimized structures. The RMS deviations either in the bond lengths or in the atomic positions are between 0.2 and 0.3 Å for the diamagnetic Cu^{III} state.

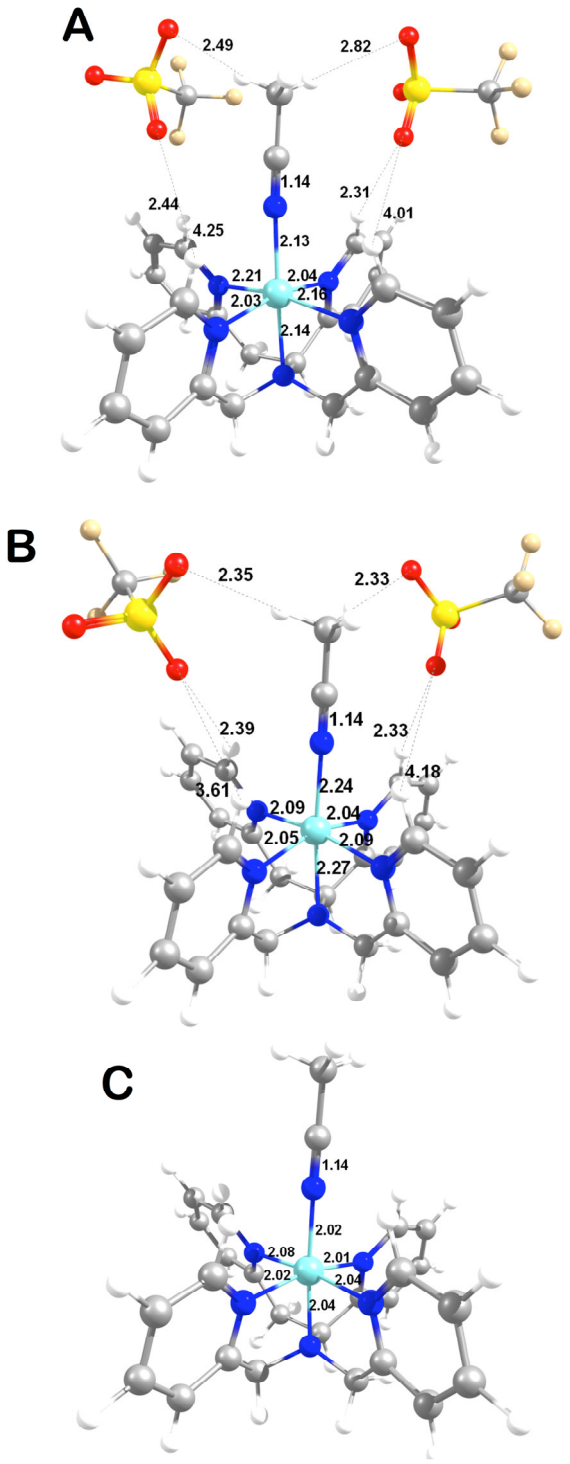

Fig. 10. Comparison of experimental (A), Cu^{II} S=1/2 with triflate counter ions (B), and Cu^{III} S=1 (C) optimized structure of complex **1** at B(38HF)P86/def2TZVP level of theory (color coding is as follows: Cu light blue, N dark blue, C gray, O red, S yellow, F light orange.

The presence of the two negative counter ions in the crystal structure unambiguously renders the formal oxidation state assignment to Cu^{II}. Thus, the preference of a Cu^{III}, S=1 centre is an artefact due to the lack of a treatment of crystal packing/environmental effects. When considering the presence of the electrostatic potential field from counter ions, the agreement for the Cu^{II} complex greatly improves (Figure 10B) as a clear indication for the critical influence of outer sphere counter ions on achieving the most accurate representation of charged coordination compounds. From the condensed phase models in Table 2, we observe a negligible difference between a low (MeCN) or high (H_2O) dielectric environment. Consideration of explicit outer-sphere triflate anions (Table 2, last columns) in gas phase or in a continuum model (Figure 10B), shows the anticipated improvements in coordination geometry due to a comprehensive capture of environmental effects. The improvement is modest when the solvent continuum is present in addition to the counter ions given that the latter captures most of the electrostatic interactions. The greater perturbation by the solute/solvent interaction for the Cu^{III} complexes is also manifested in the more than doubled heat of solvation values (-1,139 kJ mol^{-1}) compared to the Cu^{II} complex (-501 kJ mol^{-1}). The deviations of bond lengths (> 0.05 Å) and atomic position coordinates (> 0.10 Å) correspond to considerable structural differences between the experimental and optimized structures for **1** with Cu^{II} and diamagnetic Cu^{III} central ions.

Although the overall structural differences in Table 2 are within a range that can be used to differentiate among various d-electron counts, it is notable that the employed level of theory could not reproduce the axial Cu-N bonds. The Cu^{II} complex gives too long (2.24-2.27 Å, Figure 10B) while the Cu^{III} complex gives too short (2.02-2.04 Å, Figure 10C) relative to the SCXRD structure (2.13-2.14 Å, Figure 10A). In the experimentally correct charge state (Figure 10B), the triflate counter ions remain approximately at their crystallographic positions. Unexpectedly, the calculated Cu^{II} coordination environment appears to be rotated relative to the experimental structure with respect of Cu-N distances. The single unoccupied Cu $3d_x2_{-y}2$ orbital forms σ-interactions with the pyridine N centre in the calculated structure (Figure 10B) resulting in the shortest Cu-N distances of 2.04-2.09 Å. In the SCXRD structure of **1**, the longest Cu-N distances correspond to the asymmetric pyridine arm and its trans counterpart, which indicate that they may be located perpendicularly to the $3d_x2_{-y}2$ orbital.

Attempts to obtain a rotated electronic structure with a rhombic coordination environment has failed, since all calculations converged to the stationary structure as shown in Figure 10B. The rhombic distortion is likely due to additional crystal packing effects that we could not consider in the current modelling approach that was focused on molecules *versus* a periodic lattice cell.

Figure 10C shows the emergence of a close to ideal octahedral coordination environment as expected from the complete elimination of Jahn-Teller distortion forces for the paramagnetic $3d^8$ electron configuration with $t_{2g}^6 e_g^2$ 3d-manifold. The Cu-N distances now range between 2.01 and 2.08 Å, which are considerable shorter than the experimental values of 2.03-2.21 Å. Thus, we can conclude that the experimentally sound structural description can only be obtained if the correct, Cu^{II} S=1/2 formal oxidation state is considered using the B(38HF)P86/def2TZVP level of theory. Involvement of dispersion correction and a larger portion of the crystal environment in a cluster model, or consideration of a periodic model for the entire unit cell may provide a more complete structural description including the rhombic distortion. Since our goal is to clearly differentiate among various oxidation states, we proceed to eliminating the ambiguity of oxidation state assignments in **2**.

*Cu oxidation state in the mononuclear component of **2**.* The validated level of theory and modelling approach that includes treatment of environmental/outer sphere effects were employed for evaluating various oxidation state assignments for the Cu site in $[Cu(pic)_2(ClO_4)_2]$ moiety in **2**. Given the single negative charge of each ligand, this Cu complex will be anionic with a total charge ranging from -1 to -3 depending on the presence of Cu^{III}, Cu^{II}, or Cu^{I} central ion. The detailed numerical analysis for differences between the experimental and the calculated structures is given in supporting information (Table S2). Table 3 summarizes the root mean square deviations for selected bond lengths and atomic positional coordinates for the inner and outer coordination spheres.

Table 3. Root mean square deviations (Å, weighted by the number of bond lengths for each type) between B(38HF)P86/def2TZVP calculated and experimental (SCXRD) bond lengths and atomic positional coordinates in gas phase, condensed phase modeled by polarizable continuum model with water (CPCM = H_2O) parameters and including pyridinium (py^+) counter ions of the mononuclear component of **2**.

	gas phase				
	Cu^{I} [a]	Cu^{II} S=1/2	Cu^{III} S=0	Cu^{III} S=1	[b]
bond lengths	0.93	0.23	0.13	0.50	
Cu-N only	0.35	0.03	0.11	0.04	
all positions	1.15	0.70	0.58	1.34	
inner sphere	0.42	0.19	0.12	0.13	
	solvation (CPCM)				
	Cu^{I} [a]	Cu^{II} S=1/2	Cu^{III} S=0		
bond lengths	1.01	0.05	0.11		
Cu-N only	0.68	0.02	0.11		
all positions	0.93	0.26	0.13		
inner sphere	0.28	0.02	0.12		
	CPCM w/py^{+}		CPCM		
	$Cu^{(II)}$ S=1/2	$Cu^{(III)}$ S=0	$Cu^{(II)}$ SVP S=1/2	asymm. unit [c]	
bond lengths	0.02	0.11	0.02	0.08	
Cu-N only	0.02	0.11	0.02	0.03	
all positions	0.19	0.26	0.19	0.24	
inner sphere	0.02	0.12	0.08	0.09	

[a] both perchlorate ions dissociated giving a square planar four-coordinate Cu site; [b] one of the perchlorate ions dissociated giving a square pyramidal five-coordinate Cu site; [c] fragment extracted from the asymmetric unit calculations.

It speaks to the adequacy of the employed modelling approach that similar overall trends emerge for the mononuclear components of **1** and **2**. As shown in the first columns of Tables 2 and 3, the smallest RMS deviations between the experimental and calculated structures were obtained for the diamagnetic Cu^{III} formal oxidation state in gas phase models. Since the precursor of **2** is a Cu^{I} compound ($[Cu^{I}(CH_3CN)_4(ClO_4)]$, see experimental section), one could argue for residual mononuclear Cu^{I} species in **2**. However, consideration of the formal Cu^{I} oxidation state leads to dissociation of the trans, axial perchlorate ions and the formation of a square planar Cu^{I} complex, due to the Cu^{I} back-donation to the π-conjugated unoccupied frontier orbitals of the picolinate ligands. A difference to **1** was the different energy ordering

between the low and high spin Cu^{III} complexes, where the former was found to be the ground state in **2** by 21 kJ mol^{-1} due to the above mentioned back-donation. A similar stabilizing interaction is not available for the pyridine ligands in **1**. It is also evident from Table 3, that the agreement between the experimental and the paramagnetic Cu^{III} structure is as poor as for Cu^{I} due to the dissociation of one of the perchlorate anions and formation of a neutral, square pyramidal Cu^{III} coordination environment. A confinement due to the presence of a solvent cavity of a PCM model (middle section of Table 3) did not help to keep the perchlorate anions in the inner sphere coordination environment of the Cu^{I}. However, as for **1**, the Cu^{II} oxidation state gives the most reasonable structural model (Figure 11B) for the experimental structure (Figure 11A), while the agreement worsens for diamagnetic Cu^{III} complex in comparison to gas phase results.

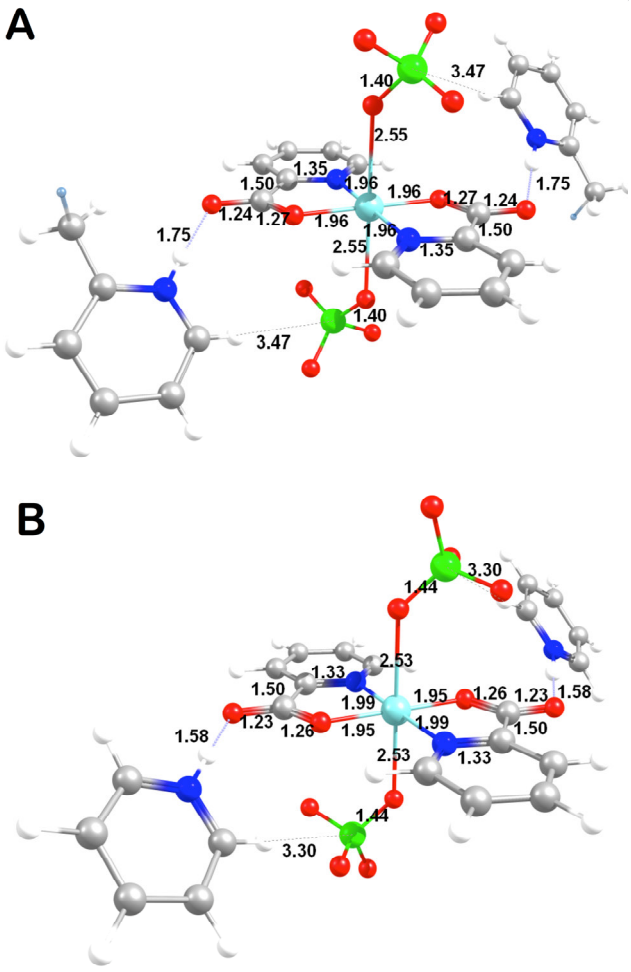

Fig. 11. Comparison of experimental (A) and Cu^{II} S=1/2 (B) optimized structure with pyridinium counter ions of the mononuclear moiety in **2** at B(38HF)P86/def2TZVP level of theory (color coding is as follows: Cu light blue, N dark blue, C gray, O red, Cl light green).

The reproduction of experimental bond lengths for the Cu^{II} centre is already excellent (within 0.05 Å in bond lengths and only 0.02 Å for the inner sphere atoms) in the continuum models. The model completeness can be enhanced by including two pyridinium ions as neutralizing cations extracted from the crystal structure. The remarkable agreement in metal-ligand bond lengths for the Cu^{II} S=1/2 state extends to the position and orientation of the pyridinium counter ions. They form strong H-bonding interactions (exp.: 1.75 Å and calc.: 1.58 Å) with the carbonyl O atoms of the picolinate ligand and weaker (exp.: 3.47 and calc.: 3.30 Å) yet non-negligible ion-dipole interactions of the C-H bond with the perchlorate anion. The formal oxidation state of Cu^{II} can be converted to an effective oxidation state by considering the atomic spin density at the Cu centre. The 0.73 e^- value from Mulliken population analysis indicate the presence of moderate ligand-to-metal electron donation for Cu-ligand bonds that is indicative of low covalency. There is insignificant (<0.01 e^-) spin density accumulation on the axial perchlorates. Each coordinated O and N centre of the picolinate ligand accumulate 0.06 and 0.08 e^- atomic spin density due to L→M donation. There is a small spin polarization of the rings and the carboxyl group indicated by atomic spin densities with alternating sign in the order of ±0.005 – ±0.009 e^-. Thus, based on both the geometric and electronic structure analyses, we can unambiguously assign the formal oxidation and spin states of the Cu centre in the mononuclear moiety in **2** to Cu^{II}. While the -2 charge of the $[Cu(picolinate)_2(ClO_4)_2]$ in **2** is not entirely unexpected, the confirmation of this assignment is essential for narrowing the oxidation state range for the trinuclear moiety of **2**. Considering the free, non-coordinated perchlorate and the solvent chlatrate in the asymmetric unit in Fig.5, we can define the total charge of the trinuclear moiety containing two picolinate ligands, two perchlorate anions, and two asymmetric N_4-chelating ligands with protonated pyridine rings to be +3. This assignment limits the total charge of the three Cu centres to be +5 with possible formal oxidation state distributions: ferro- or antiferromagnetically coupled Cu^{II}-Cu^{I}-Cu^{II} symmetric or Cu^{II}-Cu^{II}-Cu^{I} asymmetric, or the Cu^{I}-Cu^{III}-Cu^{I} symmetric and Cu^{III}-Cu^{I}-Cu^{I} asymmetric with high or low spin Cu^{III} ions.

*Investigation of the asymmetric unit of **2**.* The asymmetric unit of **2** allows for approximating the most reasonable charge and spin states of the Cu ions given its neutral molecular charge. Due to its $Cu_4C_{74}H_{67}Cl_5N_{15}O_{28}$ stoichiometry, it contains an odd number of electrons (1041 e^-), which is indicative of a paramagnetic ground state with non-integer total spin (S_t). The mononuclear moiety in **2** has been shown to contain a Cu^{II} centre with an unpaired electron (see above, Table 3 and Fig. 11). Thus, the trinuclear moiety needs to have an integer total

spin state (S_t = 0, 1, …). When the entire asymmetric unit was considered, structural optimization using the default initial guess algorithm for molecular orbitals [28] resulted in an atomic spin density distribution for the S_t = 1/2 state, where the mononuclear moiety has an unpaired electron with Cu spin density of -0.74 e^-. The trinuclear moiety shows an asymmetrical distribution of spin density with the peripheral Cu ion proximal to the mononuclear moiety and the central Cu ion have +0.73 and +0.75 e^- atomic spin densities, while the distal peripheral Cu ion is diamagnetic. The geometry optimization of this state (Figure 12A) results in asymmetric trinuclear coordination geometry, which is rather different from the symmetric SCXRD structure. The electronic structure with all Cu atomic spin densities being positive (S_t = 3/2) did not show any significant energetic or geometric differences relative to the S_t = 1/2 state. The mononuclear Cu and the central Cu sites have $3d_{x^2-y^2}$-based electron holes due to the axially elongated hexacoordinate Cu environments. The paramagnetic peripheral Cu site has a trigonal bipyramidal coordination environment with the electron hole localized on a $3d_{z^2}$ orbital. The in-plane combination of lone-pairs of the carboxylate O atoms of the picolinate connects the peripheral and central Cu sites (see the lobes in Fig. 12B). The energetic degeneracy of the S_t = 1/2 and 3/2 states indicates insignificant magnetic coupling between the mono- and trinuclear moieties. A further increase in the S_t spin number (S_t = 5/2) induces radical character on the distal pyridinium ring, as can be seen in Fig.12C. As a result of increased spin multiplicity that forces opening up ligand-based unoccupied orbitals in the S_t=5/2 state, spin density emergences on the distal peripheral site (0.76 e^-) with unchanged mononuclear Cu (0.74 e^-), proximal peripheral Cu (0.73 e^-), and central Cu (0.75 e^-) atomic spin densities. The oxidation of the previously diamagnetic distal Cu site in S_t = 3/2 state results in a 1-e^- reduction of pyridinium group, as the most electrophilic part of the asN4Py ligand. Notably, the S_t = 5/2 state is only 0.8 eV higher in energy than either of the S_t = 1/2 or 3/2 states at the B(38HF)P86/SVP/ CPCM(H_2O) level of theory. Thus, the appearance of atomic spin densities on the pyridinium ions can be taken as a direct sign of an excited state electronic structure, which will be an important criterion for evaluating the results of controlled wave function manipulations. The last column, bottom section of Table 3 includes the deviations between the SCXRD structure and the mononuclear moiety as part of the optimized asymmetric unit. The comparable values to the Cu^{II} models under similar environmental conditions further confirm its cupric charge and doublet spin state. Furthermore, it emphasizes the need of using both polarizable continuum environment and explicit pyridinium counter ions for the adequate modelling. The only notable deviation is the position of axial perchlorate ions, which move in too close to the Cu centre by 0.2 Å

relative to the SCXRD structure, thus, resulting in greater RMS values than those from isolated model structure calculations. The last two columns in Table 3 show that there is no mentionable deviation in the accuracy in going from the larger def2TZVP to a smaller SVP basis set with the exception of some angular differences that are captured in the inner sphere, atomic positional deviation values (last line in Table 3, 0.02 vs. 0.08 Å, respectively). The latter basis set is needed for avoiding computationally prohibitive situation for the trinuclear complex using the large def2TZVP basis set.

Controlled electronic structure mapping of the trinuclear component of ***2***. In order to achieve a symmetric structure for the trinuclear moiety of **2** as required by the SCXRD structure, we need to control the location of the unpaired electrons or electron holes. Merging the initial electronic structure from well-defined ionic fragments allows for systematic and reproducible mapping of various formal oxidation state and spin coupling schemes. Table 4 summarizes the relative energies and Cu atomic spin densities for all considered electronic structures. In addition to those giving total charge of +5 for the three Cu centres, we also considered alternative oxidation state assignments, as computational control to assure that experimentally unacceptable charge and spin distributions will not result in reasonable electronic structure descriptions for the trinuclear component of **2**. As an unexpected result from the controlled electronic structure calculations, we find a strong tendency for the Cu ions to adopt a formally Cu^{II} electron configuration with S_i =1/2. This is understandable, since the symmetrical electronic structure is facilitated by the symmetrical coordination environment. This is especially striking for the I+II+I assignment with a total charge of +2 and S_t = 1/2, where the spins on the peripheral Cu sites are compensated by the appearance of negative spin densities on the pyridinium rings, which is a sign of excited state electronic structure as described above for the asymmetric unit.

The lowest energy structure relative to the normal hydrogen electrode potential (4.43 eV) [29-31] was localized for the all cupric state (II+II+II assignment) with total charge of +4 and S_t = 1/2 spin state. This oxidation state assignment results in symmetric optimized structure and electron spin distribution, which would be desirable for the SCXRD structure. However, the all-cupric state cannot be the correct oxidation state assignment for the trinuclear complex in **2**, since this would require a diamagnetic, cuprous state for the mononuclear moiety. The results in Table 3 and in Figure 11 clearly indicate that a Cu^{I} oxidation state is not compatible with the hexacoordinate Cu environment for the mononuclear component of **2**.

Table 4. Summary of electronic structures calculated at B(38HF)P86/SVP level for the controlled assignments of Cu (p,p': peripheral, c: centre) oxidation and spin coupling states for the trinuclear component of **2**.

oxid. state	total charge	spin [a] coupling	S_t	ΔE_{SCF}, [b] eV	Cu^p, e^-	Cu^c, e^-	$Cu^{p'}$, e^-
I+I+I	1		0	1.0	0.000	0.000	0.000
I+II+I	2		1/2	7.1	0.723	0.745	0.723
I+III+I	3	l.s.	0	3.2	0.000	0.000	0.000
		h.s.	1	1.4	-0.729	0.758	0.729
II+I+II		f.c.	1	1.4	0.728	0.757	0.728
		af.c.	0	1.0	-0.731	0.757	0.727
II+II+I		f.c. (s)	1	1.3	-0.734	0.782	0.835
		af.c. (s)	0	1.4	-0.729	0.762	0.729
II+II+I		f.c. (as)	1	0.2	0.748	0.731	0.000
		af.c. (as)	0	0.2	0.748	-0.731	0.000
II+II+II	4	af.c.	1/2	0.0	0.731	-0.757	0.731
		f.c.	3/2	0.0	0.731	0.757	0.731
II+III+II	5	af.c.	0	26.3	-0.721	0.734	-0.722

[a] l.s. = low spin, h.s. = high spin, f.c. = ferromagnetic coupling max(Σm_s), af.c = antiferromagnetic coupling min(Σm_s), (s) symmetric structure, (as) asymmetric structure; [b] relative values include the absolute energy of a free electron 4.43 eV from normal hydrogen electrode [29-31].

Among all +3 charged states considered, the lowest energy structures were obtained for asymmetric II+II+I assignment with energetically degenerate ferromagnetically (S_t = 1) or antiferromagnetically (S_t = 0) coupled Cu centres that are only 0.2 eV higher than the structurally preferred +4 charged state with all cupric ions. The corresponding symmetrical structures are at a remarkable 1.1 and 1.2 eV higher energy level with spin density distributions that show a radicalized pyridinium ring. Even with an engineered II+II+I electronic structure, the asymmetric structure could only be obtained if the initial coordination geometry of the picolinate ligands was made asymmetric. The optimized structures with characteristic intramolecular distances are shown in Figure 13. The major structural difference due to asymmetry is the peripheral Cu-O(picolinate) distances with 0.23 Å deviation. The shorter Cu-O distance (1.94 Å) involves covalent bonding with a formally Cu^{II} site at the right hand side of Figure 13A. The central and peripheral Cu^{II}-O bonds render the carboxyl C-O bonds identical (1.25 Å), while there is about 0.03 Å difference for the Cu^{I} site

coordinated one (1.23 and 1.26 Å, the right hand side of Figure 13A). To a small extent (0.04 Å), the asymmetry is also manifested in the central Cu^{II}-O distances.

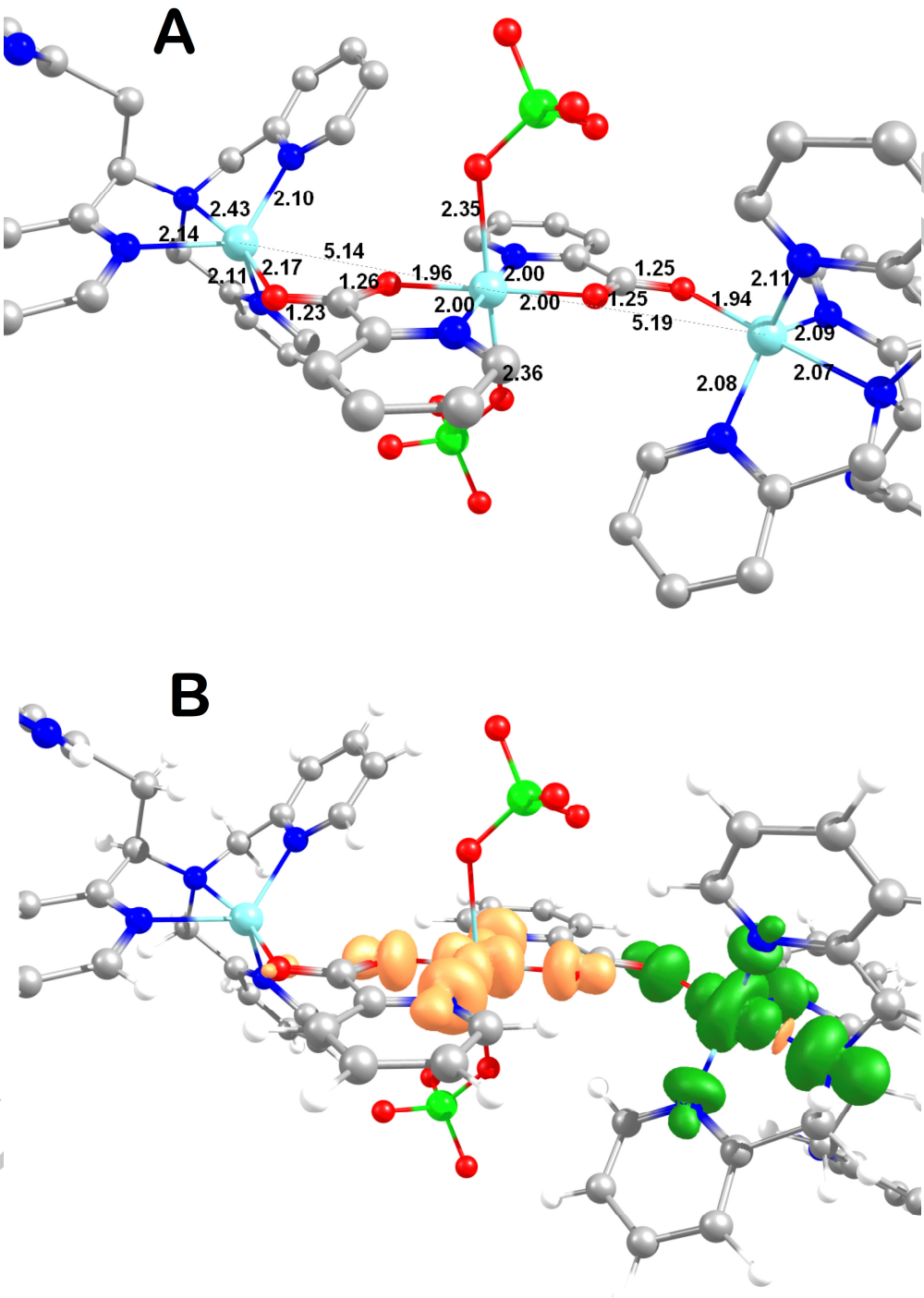

Fig. 13. Calculated lowest energy structure for the +3 charge and S_t = 1/2 spin state of the trinuclear moiety of complex **2** at B(38HF)P86/SVP/CPCM(H_2O) level of theory (A) selected bond lengths and distances in Å and (B) spin density contour plot at 0.003 e^- $Å^{-3}$ level (color coding is as follows: Cu light blue, N dark blue, C gray, O red, Cl light green).

The spin density distribution plots in Figure 13B shows the interactions of the central Cu $3d_{x}2_{-y}2$ electron hole with the in-plane combination of the picolinate carboxylate lone pair (orange lobes) and the $3d_{z}2$ electron hole on the spin polarized, peripheral Cu site with the other half of the carboxylate lone pair (green lobes). At the given level of theory, we see insignificant energetic and structural differences between the ferro- and antiferromagnetically-coupled states. All calculations indicate insignificant magnetic interactions among the Cu sites through the 1,3-bridged picolinate carboxylate groups. The spin states S_t = 1/2 and 3/2 states in the asymmetric unit, S_t = 0 and 1 states in the asymmetric trinuclear moiety, and the S_t = 1/2 and 3/2 states for the symmetric II+II+II assignment (Table 4) are energetically degenerate.

Thus, we can consider the trinuclear complex to be held together by dominantly ionic and small, but non-negligible covalent interactions. The modest degree of covalency can be estimated from the at most 0.27 e^- deviation in Cu spin densities from the ionic cupric limit. In other words, each N/O ligands donates approximately 0.06±0.01 e^- to the Cu sites. In the light of the electronic structure analyses and structural optimizations, we conclude that complex **2** is best described by a linear combination of two asymmetric resonance structures that alternate between Cu^{II}- Cu^{II}- Cu^{I} and Cu^{I}- Cu^{II}- Cu^{II} states.

3. Experimental Section

Materials. All syntheses were done in Ar atmosphere unless stated otherwise. Solvents used for the synthesis and reactions were purified by standard methods and stored under Ar. All chemicals for the synthesis were purchased from Sigma-Aldrich and used without further purification.

Instrumentation. The crystal evaluation and intensity data collection for **1** and **2** were performed on a Rigaku Oxford Diffraction SuperNova diffractometer using Cu K radiation (= 1.54184 Å) at 173 K. Crystallographic data and selected bond lengths and angles are listed in Tables 5 and 6, whereas their structures are displayed in Figures 1 and 5. SHELX–2013 was used for structure solution and full matrix least squares refinement on F^2 [32]. The UV-visible spectra were recorded on an Agilent 8453 diode-array spectrophotometer using quartz cells. Cyclic voltammetry measurements were carried out on a VoltaLab 10 potentiostat with VoltaMaster 4 software for data processing. The electrodes were as follows: glassy carbon (working), Pt (auxiliary), and Ag/AgCl in 3 M KCl. The potentials were referenced vs. the ferrocene/ferrocenium (Fc/Fc^+) redox couple. IR spectra were recorded using a Thermo Nicolet Avatar 330 FT-IR instrument (Thermo Nicolet Corporation,

Madison, WI, USA). Samples were prepared in the form of KBr pellets. ESI-MS samples were analysed using triple quadruple Micromass Quattro spectrometer (Waters, Milford, MA, USA) that was operated in both positive and negative electrospray ionization mode. EPR spectra were recorded with a BRUKER EleXsys E500 spectrometer at room temperature (microwave frequency 9.81 GHz, microwave power 13 mW, modulation amplitude 5 G, modulation frequency 100 kHz). Powder samples were measured in quartz EPR tubes. Compounds were dissolved in acetonitrile and isotropic EPR spectra were measured in capillary. Isotropic EPR spectra were simulated with the "EPR" program [33]. The linewidths was described by the help of relaxation parameters α, β, γ through the equation $\sigma_{MI}=\alpha+\beta M_I+\gamma M_I^2$, where M_I denotes the magnetic quantum number of copper nucleus. Since a natural $CuCl_2$ was used for the measurements, the spectra were calculated as the sum of the spectra of ^{63}Cu and ^{65}Cu weighted by their natural abundances. The copper and nitrogen coupling constants and the relaxation parameters were obtained in field units (Gauss = 10^{-4} T).

Dioxygen uptake. 0.04 mmol $Cu^{I}(CH_3CN)_4ClO_4$, 0.02 mmol asN4Py and 0.04 mmol 2-pyridinecarboxaldehyde were mixed in 1.5 ml acetonitrile in a reactor vessel connected to a gas burette. Dioxygen was bubbled through the solvent prior to the experiment. The properly sealed 50 ml gas burette was filled with pure dioxygen. The dioxygen uptake was measured by gas volumetry as a function of time on minutes time scale by taking into account pressure and volume at 303 K.

*Synthesis of $[Cu^{II}(asN4Py)(MeCN)](OTf)_2$ (**1**)*. 0.100 g (0.26 mmol) asN4Py ligand, and 0.095 g (0.26 mmol) $Cu^{II}(OTf)_2$ were dissolved in 3 ml dry MeCN under Ar atmosphere. The solution was stirred at r.t. for two hours. Dry diethyl ether was layered onto the clear blue solution and it was placed to the freezer (-20°C). Blue crystals formed during overnight. Yield: 0.145 g (67 %).

FT-IR (KBr, cm^{-1}): 3089 w, 2925 w, 1608 m, 1573 w, 1481 w, 1445 w, 1274 s, 1260 s, 1225 m, 1162 s, 1030 s, 766 m, 638 s, 574 w, 517 w. UV–Vis (MeCN) λ_{max}(log ε, $dm^3mol^{-1}cm^{-1}$): 256 (4.22), 630 (1.89), 852 (2.10). EPR: g_0 = 2.1223(2), A_0 = 54.6(2) G, α = 51.4(5) G, β = -6.4(2) G, γ = -0.2(1) G.

*Synthesis of $[Cu^{II}(pic)_2(ClO_4)_2][Cu_3(asN4Py)_2(pic)_2(ClO_4)_2](ClO_4)$ (**2**)*. 0.100 g (0.26 mmol) asN4Py ligand, 25 µl (0.26 mmol) 2-pyridinecarboxaldehyde and 0.086 g (0.26 mmol) $[Cu^{I}(CH_3CN)_4](ClO_4)$ were dissolved in 1.5 ml MeCN under O_2 (or $^{18}O_2$). The solution was stirred at r.t. for one hour. After reaction, the solvent was removed by rotavapor. The crude

green powder was washed with diethyl ether. Cubic shaped green crystals formed in dry MeCN after two nights. Yield: 0.144 g (55 %).

FT-IR (KBr, cm^{-1}): 3434 m, 3077 w, 2925 w, 1712 w, 1628 m, 1607 s, 1590 s, 1571 m, 1477 s, 1440 s, 1386 w, 1358 w, 1294 w, 1143 sh, 1090 vs, 1022 m, 1022 m, 767 s, 624 s. UV–Vis (MeCN) max(log , $dm^3mol^{-1}cm^{-1}$): 257 (4.56), 670 (2.31), 851 (2.42).

Table 5. Summary of crystal data and intensity collection and structure refinement parameters for **1** and **2**.

Compound	**1**	**2**
Chemical formula	$C_{28}H_{26}CuF_6N_6O_6S_2$	$C_{38}H_{35}Cl_3Cu_2N_8O_{16}$
Formula weight	784.21	1093.17
Crystal system	monoclinic	triclinic
Space group	P 2_1/n	P -1
a (Å)	12.7184(10)	10.9037(3)
b (Å)	19.4461(15)	12.7500(3)
c (Å)	13.0224(11)	17.1221(5)
α(°)	90	99.616(2)
β(°)	92.3626(8)	108.277(3)
γ(°)	90	97.967(2)
Volume ($Å^3$)	3218.00(5)	2181.64(11)
Z	4	2
Calc. dens. (g cm^{-1})	1.619	1.664
Temperature (K)	173(10)	173(10)
Abs. coeff. (mm^{-1})	2.958	3.607
F (0 0 0)	1596	1112
Obs. reflections	5947	8218
Goodness-of-fit	1.062	1.021
R_1 (obs.)	0.0624	0.0578
wR_2 (obs.)	0.1539	0.1282

Table 6. Selected bond distances (Å) and angles (°) for **1** and **2**.

distances (in **1**)		angles (in **1**)	
Cu(1) – N(1)	2.028(2)	N(1)-Cu(1)-N(2)	82.32(10)
Cu(1) – N(2)	2.059(3)	N(2)-Cu(1)-N(3)	113.14(10)
Cu(1) – N(3)	2.099(3)	N(2)-Cu(1)-O(1)	101.53(10)
Cu(1) – N(4)	2.042(2)	N(3)-Cu(1)-N(4)	110.17(10)
Cu(1) – O(1)	1.945(2)	N(6)-Cu(2)-O(2)	96.63(10)
Cu(2) – O(2)	1.968(2)	O(2)-Cu(2)-O(2)	180.00(11)
Cu(2) – N(6)	1.961(3)	N(6)-Cu(2)-N(6)	180.00(14)
distances (in **2**)		angles (in **2**)	
Cu(1) – N(1)	2.138(3)	N(1)-Cu(1)-N(2)	81.6(1)
Cu(1) – N(2)	2.163(3)	N(2)-Cu(1)-N(3)	89.8(1)
Cu(1) – N(3)	2.032(3)	N(2)-Cu(1)-N(4)	89.2(1)
Cu(1) – N(4)	2.039(3)	N(2)-Cu(1)-N(6)	95.8(1)
Cu(1) – N(5)	2.213(3)	N(2)-Cu(1)-N(5)	167.6(1)
Cu(1) – N(6)	2.130(3)	N(1)-Cu(1)-N(6)	177.3(1)

Computational modelling. Three structural models were considered for systematically evaluating the Cu oxidation and spin state dependence of ground state electronic structure*s* and optimized molecular geometries. The atomic positions and selected bond lengths considered during the geometric structural analysis are summarized in Figure 14. The entire asymmetric unit as shown in Fig.14D with a neutral charge provided a well-defined reference composition. The oxidative conditions employed in synthesizing **2** starting from a Cu^{I} precursor ($[Cu^{I}(CH_3CN)_4](ClO_4)$) allow for considering a range of possible oxidation states for the Cu centres from Cu^{I} through Cu^{II} with S=1/2 spin ($1e^-$ oxidized centre) to Cu^{III} with S=1 high spin (HS) or S=0 low spin (LS) ($2e^-$ oxidized centre) states. These Cu oxidation and spin states, and their various ferro- and antiferromagnetic spin coupling schemes give a range of combinations that we explored using broken-symmetry, density functional theory electronic structure calculations and structural optimizations. The selected level of theory was the spectroscopically calibrated B(38HF)P86 set of functionals with saturated basis set that has been shown to perform well for both ground and excited states of Cu complexes [14] and bioinorganic compounds [13], metalloprotein [17] and metalloenzyme Cu sites [14,16]. For

all models (Figs.14A-C) except the asymmetric unit (Fig.14D), the all electron def2TZVP [34,35] triple-ζ quality basis set with polarization functions were utilized. Due to the size of the computational model (193 atoms and 1041 electrons), the asymmetric unit was treated using a smaller, but still acceptably saturated SVP [34,35] basis set. Atomic spin density distributions were obtained from the Mulliken population analysis and spin density plots were created from cube files of spin density at 0.003 e^- Å^{-3} contour levels in ChemCraft [36]. All initial and optimized structures are provided as supporting information (see pages 7-20).

While we did not carry out periodic boundary condition calculations for the entire unit cell; we considered outer-sphere environmental effects *in lieu* of crystal packing forces, such as aqueous and acetonitrile solvent environments through COSMO [37,39] polarizable continuum environment with dielectric constants of 80 and 36.7, respectively, and presence of explicit perchlorate, trifluoromethylsulfonate, and pyridinium counter ions.

Most structural optimizations were initiated from the crystal structure that we compare to the optimized structures; thus, we always added optimization steps after obtaining a stationary point by applying random displacements of all atoms in the [-0.2, 0.2] range. The shaking of stationary structures was repeated until no lower energy structure was found. All calculations were carried out using Gaussian09 Revision D01 suite of programs [40]. In addition to using the built in initial guess algorithm [28], we have employed the ionic fragment approach [41] to reproducibly construct the initial electronic structure from well-defined ionic fragments such as Cu^{I}, Cu^{II} S=1/2, Cu^{III} S=0, Cu^{III} S=1, $(picolate)^-$, $(perchlorate)^-$, acetonitrile solvent, and the protonated asN4Py ligand with pyridinium groups.

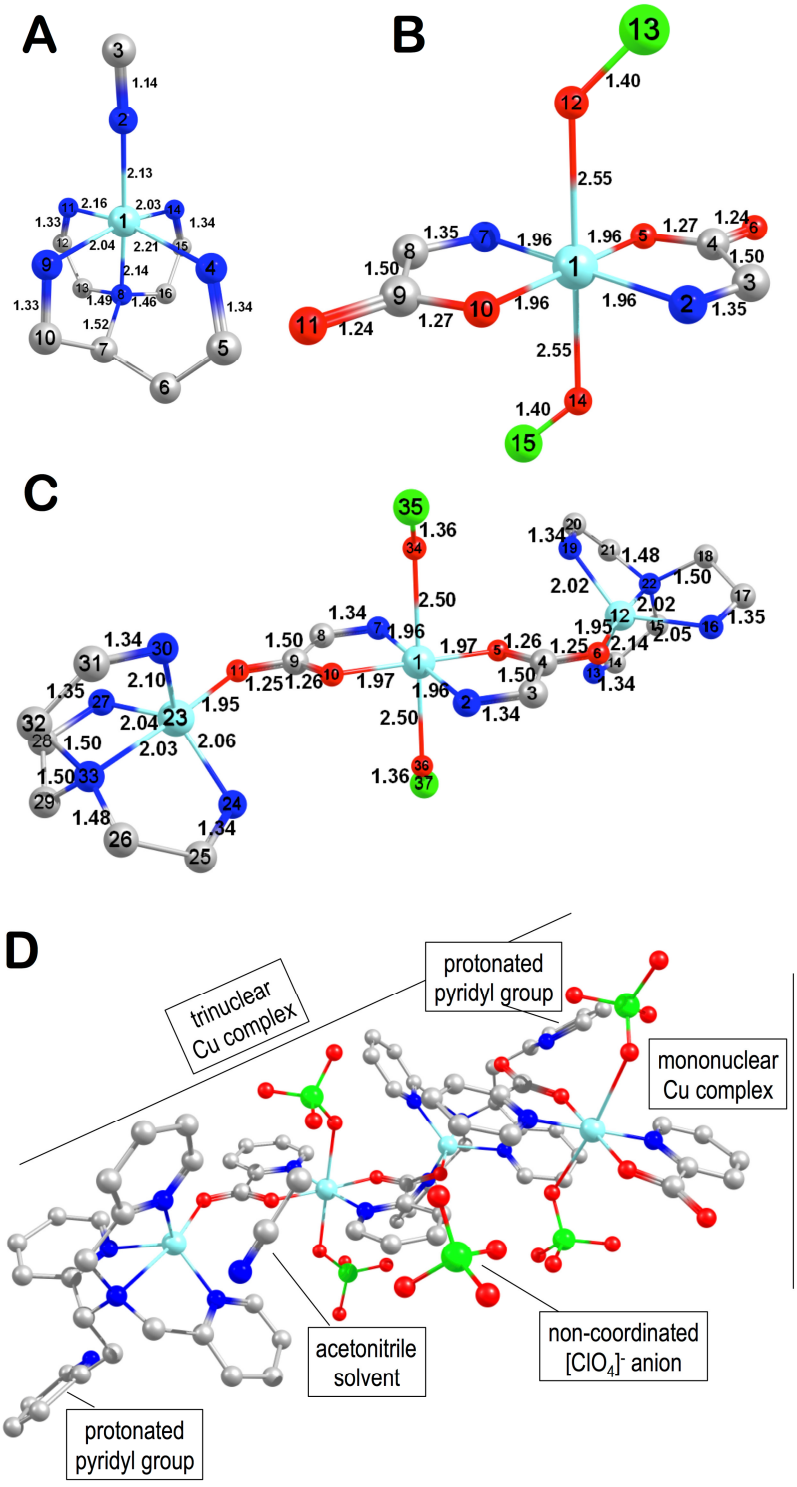

Fig. 14. Overview of selected atoms and environments considered in computational modelling (A): **1** (B): mononuclear Cu component of **2** (C): trinuclear Cu component of **2** (D): entire asymmetric unit of **2** (colour coding is as follows: Cu light blue, N dark blue, C gray, O red, Cl light green).

4. Conclusions

Chiral copper complexes have been synthesized using the modified N4Py ligand (asN4Py) with the aim of employing them in biomimetic applications, such as enantioselective oxidation processes, as synthetic models of copper containing enzymes. In the presence of pyridinecarboxaldehyde and O_2 oxidant the precursor Cu^{I} salt formed a unique polynuclear complex where formal oxidation states of the copper centres were remained obscured in the XRD measurements. Using a systematic computational mapping of possible oxidation and spin states, we unexpectedly found evidence for valence localization from spectroscopically validated hybrid density functional theory that suggests the presence of two asymmetric resonance structures in the unit cell. Simultaneous presence of the formally Cu^{II}-Cu^{II}-Cu^{I} and Cu^{I}-Cu^{II}-Cu^{II} states in energetically degenerate antiferromagnetic or ferromagnetic state gives an average symmetric structure as manifested by the single crystal X-ray diffraction structure.

Acknowledgements

This work was supported by a grant from The Hungarian Research Fund (OTKA) K108489, the Hungarian Academy of Sciences through a János Bólyai Scholarship (R. Csonka), and the New National Excellence Program of the Ministry of Human Capacities-2016-3-IV. (D. Lakk-Bogáth), COST Actions CM1205, CM1201, and CM1003. RKSz acknowledges the computational resources from the Hyalite High Performance Computing facility at Montana State University.

Appendix A. Supplementary material

‡ Deposited CIF file: CCDC 1516132 and 1516133. Optimized atomic positional coordinates for all models and the comparison of internal coordinates to experimental structures.

References

[1] A. R. McDonald and Q. J. L., Coord. Chem. Rev. 257 (2013) 414.

[2] J. Chen, Y.-M. Lee, K.M. Davis, X. Wu, M.S. Seo, K.-B. Cho, H. Yoon, Y.J. Park, S. Fukuzumi, Y.N. Pushkar and W. Nam, J. Am. Chem. Soc. 135 (2013) 6388.

[3] D. Wang, K. Ray, M.J. Collins, E.R. Farquhar, J.R. Frisch, L. Gómez, T.A. Jackson, M. Kerscher, A. Waleska, P. Comba, M. Costas and L. Que Jr., Chem. Sci. 4 (2013) 282.

[4] J. Hohenberger, K. Ray and K. Meyer, Nat. Commun. 3 (2012) 720.

[5] S.V. Kryatov, S. Taktak, I.V. Korendovych, E.V. Rybak-Akimova, J. Kaizer, S. Torelli, X. Shan, S. Mandal, V.L. MacMurdo, A.M. Payeras and L. Que Jr, Inorg. Chem. 44 (2005) 85.

[6] H.-F. Hsu, Y.H. Dong, L. Shu, V.G. Young Jr. and L. Que Jr., J. Am. Chem. Soc. 121 (1999) 5230.

[7] M. Lubben, A. Meetsma, E.C. Wilkinson, B. Feringa and L. Que Jr., Angew. Chem. Int. Ed. Engl. 34 (1995) 1512.

[8] Y.O. Lyakin and A.A. Shteinman, Kinet. Catal. 53 (2012) 694.

[9] D. Lakk-Bogáth, R. Csonka, G. Speier, M. Réglier, A.J. Simaan, J.-V. Naubron, M. Giorgi, K. Lázár and J. Kaizer, Inorg. Chem. 55 (2016) 10090.

[10] T. Punniyamurthy and L. Rout, Coord. Chem. Rev. 252 (2008) 134.

[11] K.B. Szpalolski, K. Latham, C.J. Rix and J.M. White, Inorg. Chim. Acta 376 (2011) 628.

[12] D. Lakk-Bogáth, G. Speier and J. Kaizer, New J. Chem. 39 (2015) 8245.

[13] A. Szorcsik, F. Matyuska, A. Benyei, N.V. Nagy, R.K. Szilagyi and T. Gajda, Dalton Trans. 45 (2016) 14998-15012.

[14] R.K. Szilagyi, M. Metz and E.I. Solomon, J. Chem. Phys. A 106 (2002) 2994-3007.

[15] R.K. Szilagyi and E.I. Solomon, Current Op. Chem. Biol. 6 (2002) 250-258.

[16] D. Rokhsana, A.E. Howells, D.M. Dooley and R.K. Szilagyi, Inorg. Chem. 51 (2012) 3513-3524.

[17] T. Yamaguchi, J. Yano, Y. Vittal, Y. Nihei, H. Togashi, R.K. Szilagyi and T. Kohzuma, Bulletin of the Chemical Society of Japan 88 (2015) 1642-1652.

[18] W.K.C. Lo, C.J. McAdam, A.G. Blackman, J.D. Crowley and D.A. McMorran, Inorg. Chim. Acta 426 (2015) 183.

[19] M.A.S. Goher, A.K. Hafez, M.A.M. Abu-Youssef, A. Popitsch, H.P. Fritzer and F.A. Mautner, Monat. Chem. 125 (1994) 833.

[20] A.B.P. Lever, Inorganic Electronic Spectroscopy, Elsevier Science, Amsterdam, Netherlands, 2nd edn., 1984.

[21] A.W. Addison, T.N. Rao, J. Reedijk, J. van Rijn and G.C. Verschoor, J. Chem. Soc., Dalton Trans. (1984) 1349.

[22] A. Colette, A.M. Ondoh, D.M. Yufanyi and D.S.Y. Gaelle, Int. J. Chem. 7 (2015) 10.

[23] B. Zurowska, J. Mrozinski and Z. Ciunik, Polyhedron 26 (2007) 1251.

[24] T. Murakami, S. Hatakeyama, S. Igarashi and Y. Yukawa, Inorg. Chim. Acta 310 (2000) 96.

[25] C.-X. Zhang, Y.-Y. Zhang and J. Sheng, J. Coord. Chem. 58 (2005) 189.

[26] N.M.N. Gowda, S.B. Naikar and G.K.N. Reddy, Adv. Inorg. Chem. 28 (1984) 255.

[27] B. Golec, P. Das, M. Bahou and Y.-P. Lee, J. Phys. Chem. A, 117 (2013) 13680.

[28] J. Harris, Phys. Rev. B 31 (1985) 1770.

[29] S. Trasatti, Pure Appl. Chem. 58 (1986) 955.

[30] W.R. Fawcett, Langmuir 24 (2008) 9868.

[31] A.A. Isse and A. Gennaro, J. Phys. Chem. B 114 (2010) 7894.

[32] G.M. Sheldrick, Acta Cryst. A64 (2008) 112.

[33] A. Rockenbauer, L. Korecz, Appl. Magn. Reson. 10 (1996) 29.

[34] A. Schäfer, H. Horn and R. Ahlrichs, J. Chem. Phys. 97 (1992) 2571.

[35] A. Schäfer, C. Huber and R. Ahlrichs, J. Chem. Phys. 100 (1994) 5829.

[36] G. Andrienko, ChemCraft Visualizer Revision 1.8 Built 489, http://www.chemcraftprog.com, 2016.

[37] A. Klamt, Wiley Interdisciplinary Reviews-Computational Molecular Science, 2011, 1, 699.

[38] V. Barone and M. Cossi, J. Phys. Chem. A 102 (1998) 1995.

[39] M. Cossi, N. Rega, G. Scalmani and V. Barone, J. Comp. Chem. 24 (2003) 669.

[40] M.J. Frisch, G.W. Trucks, H.B. Schlegel, G.E. Scuseria, M.A. Robb, J.R. Cheeseman, G. Scalmani, V. Barone, B. Mennucci, G.A. Petersson, H. Nakatsuji, M. Caricato, X. Li, H.P. Hratchian, A.F. Izmaylov, J. Bloino, G. Zheng, J.L. Sonnenberg, M. Hada, M. Ehara, K. Toyota, R. Fukuda, J. Hasegawa, M. Ishida, T. Nakajima, Y. Honda, O. Kitao, H. Nakai, T. Vreven, J.A. Montgomery, Jr., J.E. Peralta, F. Ogliaro, M. Bearpark, J.J. Heyd, E. Brothers, K.N. Kudin, V.N. Staroverov, R. Kobayashi, J. Normand, K. Raghavachari, A. Rendell, J.C. Burant, S.S. Iyengar, J. Tomasi, M. Cossi, N. Rega, N.J. Millam, M. Klene, J.E. Knox, J.B. Cross, V. Bakken, C. Adamo, J. Jaramillo, R. Gomperts, R.E. Stratmann, O. Yazyev, A.J. Austin, R. Cammi, C. Pomelli, J.W. Ochterski, R.L. Martin, K. Morokuma, V.G. Zakrzewski, G.A. Voth, P. Salvador, J.J. Dannenberg, S. Dapprich, A.D. Daniels, Ö. Farkas, J.B. Foresman, J.V. Ortiz, J. Cioslowski and D.J. Fox, Gaussian09 Revision D.01, Gaussian, Inc., Wallingford CT, 2009.

[41] R.K. Szilagyi and M. Winslow, J. Comp. Chem. 27 (2006) 1385.

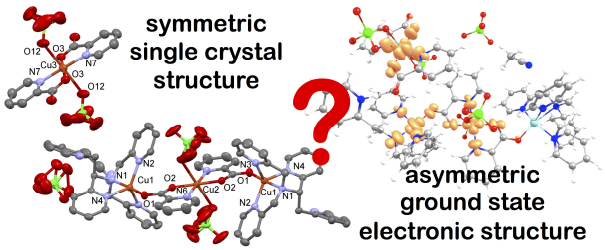

Non-innocent oxidation chemistry of a Cu(I) complex with chiral ligand environment gives a trinuclear complex with ambiguous oxidation state assignment.

Highlights :

Mono and trinuclear copper complexes were synthesized by chiral polypyridyl ligand.

The structures were elucidated by single crystal X-ray diffraction and spectroscopic methods.

The non-trivial assignments of the formal Cu oxidation states were made by hybrid density functional theory.

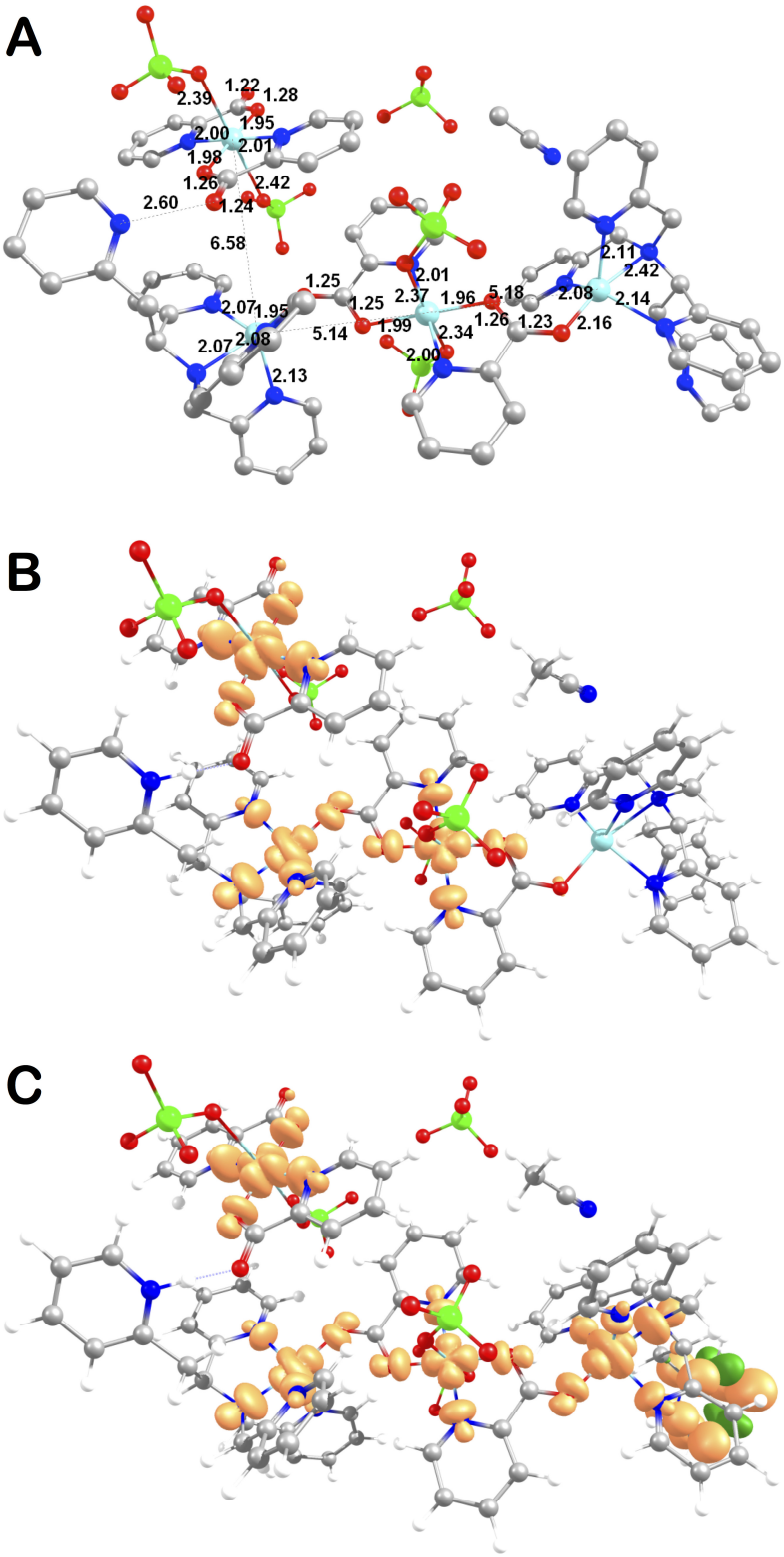

Fig. 12